Chemical Science

ROYAL SOCIETY OF CHEMISTRY

EDGE ARTICLE

View Article Online
View Journal | View Issue

Open Access Article. Published on 04 November 2024. Downloaded on 9/9/2025 4:14:33 AM. This article is licensed under a Creative Commons Attribution-NonCommercial 3.0 Unported Licence.

Check for updates

Cite this: *Chem. Sci.*, 2024, **15**, 19556

All publication charges for this article have been paid for by the Royal Society of Chemistry

Received 7th August 2024
Accepted 3rd November 2024

DOI: 10.1039/d4sc05286b

rsc.li/chemical-science

Three in one: engineering MOF channels *via* coordinated water arrays for regulated separation of alkanes and alkenes†

Lu-Lu Ma,[ab] Pavel N. Zolotarev,[c] Kang Zhou,[b] Xin Zhou,[b] Jiaqi Liu,[b] Jiafeng Miao,[b] Shenfang Li,[b] Guo-Ping Yang, *[a] Yao-Yu Wang, [a] Davide M. Proserpio, *[c] Jing Li *[db] and Hao Wang *[b]

Purifying alkenes (mainly ethylene and propylene) by removing their corresponding alkanes is crucial yet challenging in the chemical industry. Selective physisorption shows promise for effective separation but demands precise pore dimensions and/or pore chemistry of adsorbents. We report an yttrium-based metal–organic framework, $Y_2(TCHB)(OH)_2 \cdot 2H_2O$ (**HIAM-317**, TCHB = 3,3′,5,5′-tetrakis(4-carboxyphenyl)-2,2′,4,4′,6,6′-hexamethyl-1,1′-biphenyl), that can separate ethylene/ethane and propylene/propane *via* mechanisms regulated by coordinated water arrays. In the presence of coordinated water arrays, **HIAM-317** sieves alkanes from alkenes. When fully activated by removing coordinated water arrays, it selectively adsorbs ethane over ethylene and propylene over propane. This separation ability has been experimentally verified, and the underlying mechanism was uncovered through theoretical calculations and modeling.

Introduction

Ethylene and propylene are key chemical feedstocks for the production of plastics and high-value chemicals.[1–3] In 2023, the global production of ethylene and propylene are 220 and 130 million metric tons, respectively, growing at an annual rate of 5.50%.[4] Steam cracking serves as the primary method for producing ethylene and propylene, where unwanted by-products including alkanes are also generated. The subsequent purification of alkenes from alkanes currently relies heavily on energy-intensive cryogenic distillation processes.[5–7] The substantial energy input required for alkene purification process contributes significantly to global energy consumption, positioning it among the seven chemical separations to change the world.[8–10]

The separation of alkenes and alkanes by selective physisorption using porous solids has attracted tremendous attention due to its great potential for energy-efficient alkene purification under mild conditions.[11–13] The key to achieve efficient adsorptive separation lies in the development of adsorbents with the desired separation mechanism and optimal separation efficiency.[14–16] In general, physisorbents discriminate alkenes and alkanes relying on appropriate pore dimensions for kinetically-driven molecular sieving, or optimal pore surface chemistry for thermodynamically-driven selective adsorption.[17–19] The subtle difference in the physicochemical properties of alkenes and alkanes present a formidable challenge for their effective separation. Achieving high selectivity imposes stringent requirements on pore dimensions and/or pore surface chemistry of adsorbents, particularly for complete molecular exclusion or reversed alkane-selective separation.[20–22]

Compared to traditional inorganic adsorbents such as zeolites and organic adsorbents such as carbons, polymers, covalent organic frameworks (COFs), and hydrogen-bonded organic frameworks (HOFs), metal–organic frameworks (MOFs) excel in separating physicochemically similar molecules because of their intrinsic features, including diverse structures, highly controllable pore dimensions and functionality.[23–25] In particular, successful practice of reticular chemistry has enabled chemists to precisely tailor the pore structure for desired separation.[26,27] Over the past decade, intensive studies

[a]*Key Laboratory of Synthetic and Natural Functional Molecule Chemistry of the Ministry of Education, Shaanxi Key Laboratory of Physico-Inorganic Chemistry, College of Chemistry & Materials Science, Northwest University, Xi'an 710127, P. R. China. E-mail: ygp@nwu.edu.cn*

[b]*Hoffmann Institute of Advanced Materials, Shenzhen Polytechnic, 7098 Liuxian Blvd., Nanshan District, Shenzhen, Guangdong 518055, P. R. China. E-mail: wanghao@szpt.edu.cn*

[c]*Dipartimento di Chimica, Università; degli Studi di Milano, 20133 Milano, Italy. E-mail: davide.proserpio@unimi.it*

[d]*Department of Chemistry and Chemical Biology, Rutgers University, 123 Bevier Road, Piscataway, New Jersey 08854, USA. E-mail: jingli@rutgers.edu*

† Electronic supplementary information (ESI) available: Experimental methods, PXRD analysis, TGA curves, additional adsorption isotherms, and calculation of adsorption selectivity and heat. CCDC 2340289 (**HIAM-317**) and 2340290 (**HIAM-317a**). For ESI and crystallographic data in CIF or other electronic format see DOI: https://doi.org/10.1039/d4sc05286b

© 2024 The Author(s). Published by the Royal Society of Chemistry

Open Access Article. Published on 04 November 2024. Downloaded on 9/9/2025 4:14:33 AM. This article is licensed under a Creative Commons Attribution-NonCommercial 3.0 Unported Licence.

have been focused on fine-tuning of MOF pore aperture for full sieving of alkenes over alkanes, or elaborate engineering of pore surface chemistry for targeted selective recognition of alkanes over alkenes. The current state-of-the-art MOFs separate alkenes and alkanes *via* three mechanisms: kinetic sieving, thermodynamically alkene-selective, and thermodynamically alkane-selective (reversed separation).[28,29] It is important to note that each of the three mechanisms has pros and cons, and each of them can be optimal for practical implementation depending on application conditions (*e.g.*, mixture compositions, separation temperature, impurities, *etc.*). Among the various adsorbents studied, the majority follow a single separation mechanism, and it remains challenging and relatively unexplored to engineer adsorbent structures for controllable and adaptable separation behaviour, especially on a single adsorbent (Fig. 1). This is critical for disclosing the relations between the pore structure of the adsorbents and their selective adsorption behaviour, and for rational design of desirable adsorbents for high performance separation of alkenes and alkanes.

In this work, we synthesized an yttrium-based MOF, $Y_2(TCHB)(OH)_2 \cdot 2H_2O$ (**HIAM-317**, HIAM stands for Hoffmann Institute of Advanced Materials), with coordinated water arrays along its one-dimensional channels, which act as a regulatory factor of its pore dimensions and pore surface chemistry. When activated at relatively low temperature with coordinated water molecules remaining intact, the pore aperture of the MOFs is defined by these water arrays enabling the splitting of both ethylene/ethane and propylene/propane. As the activation temperature increases and coordinated water molecules are removed, the accessible pore aperture expands significantly, allowing all alkenes/alkanes (C2 and C3) to diffuse freely along the open channel. However, the surface chemistry of the expanded channel exhibits adsorbate-dependent molecular recognition, favoring adsorption of ethane over ethylene and propylene over propane. The separation capabilities of **HIAM-317** with and without coordinated water arrays have been validated experimentally by breakthrough measurements of alkene/alkane mixtures. Furthermore, the role of coordinated water arrays in regulating the pore dimensions and pore surface chemistry is verified by DFT calculations and molecular modelling, which also offer insights into the underlying separation mechanisms.

Results and discussion

Crystal structure

The solvothermal reaction of $Y(NO_3)_3 \cdot 6H_2O$ with H_4TCHB [3,3′,5,5′-tetrakis(4-carboxyphenyl)-2,2′,4,4′,6,6′-hexamethyl-1,1′-biphenyl] in *N*,*N*′-dimethylformamide (DMF) yielded block-shaped crystals of **HIAM-317** (Fig. S1†). Single-crystal X-ray diffraction (SCXRD) analysis revealed that it crystallizes in the orthorhombic crystal system with a space group of *Ibam*. In the crystal structure of **HIAM-317**, the asymmetric unit contains a nine-coordinated Y^{3+} ion bonded to half of the $TCHB^{4-}$ linker and a water molecule (Fig. S6†). Each central Y^{3+} ion in the structure is surrounded by nine oxygen atoms, with six of them from the carboxyl groups of $TCHB^{4-}$, two bridging OH^-, and one terminal water molecule. The bond length of $Y–O_{water}$ is 2.336(4) Å, slightly longer than that of $Y–O_{OH^-}$ (2.258–2.317 Å), suggesting a weaker bonding between water molecules and the central Y^{3+}, and removal of the coordinated water can potentially create an open Lewis acid active site. Adjacent Y^{3+} ions are interconnected by the carboxylate groups from $TCHB^{4-}$ linkers, forming one-dimensional (1D) Y-based chains along the crystallographic *c*-axis (Fig. 2a). The infinite rod-like Y–O chains serve as secondary building units (SBUs) which are propagated through $TCHB^{4-}$ struts, forming a three-dimensional (3D) framework containing 1D channels (Fig. 2c). Notably, the coordinated water molecules form 1D arrays along the channels, contracting the accessible pore aperture of the material.

We applied a detailed topological analysis of **HIAM-317** using both standard and cluster representations as implemented in ToposPro[30] following IUPAC suggestions.[31] Analysis

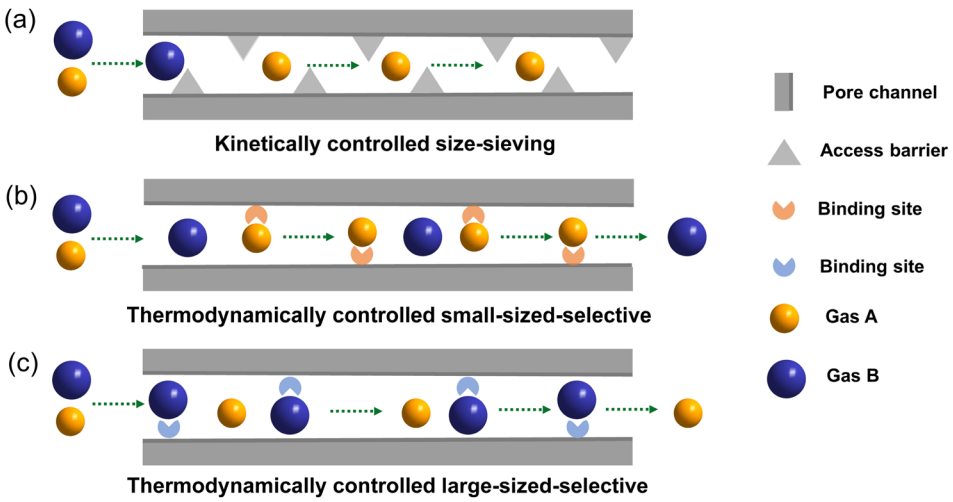

Fig. 1 Schematic diagram of the three separation mechanisms practiced in this work: (a) kinetically controlled size-sieving, (b) thermodynamically controlled small-sized-selective, (c) thermodynamically controlled large-sized-selective.

Open Access Article. Published on 04 November 2024. Downloaded on 9/9/2025 4:14:33 AM.
This article is licensed under a Creative Commons Attribution-NonCommercial 3.0 Unported Licence.

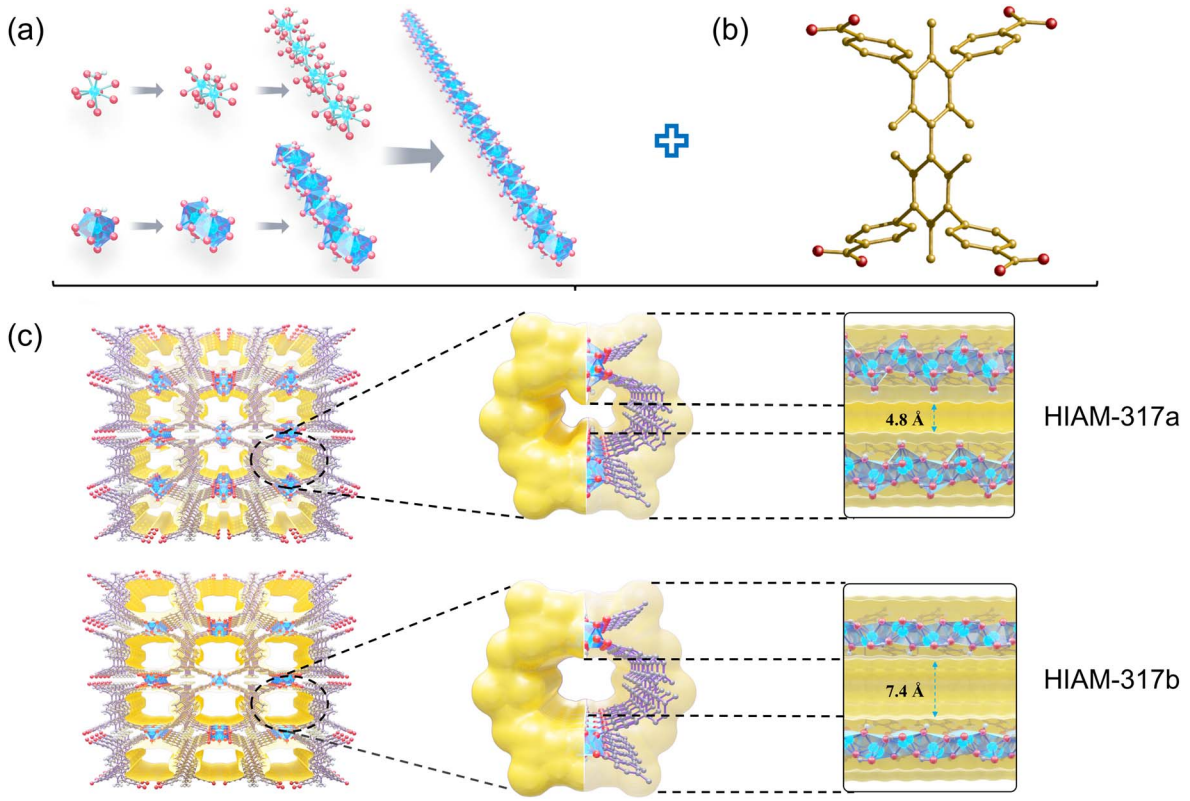

Fig. 2 (a) The 1D chain SBU of **HIAM-317**; (b) organic ligand H_4TCHB; (c) the 3D framework structure and channel environment of **HIAM-317a** and **HIAM-317b** (view from *a* direction). Color code: Y, blue; O, red; C, gray or golden; H, white.

by applying the standard representation, in which metal ions and ligand's center of mass serve as network nodes, results in the 6,8-connected **sea** net (with the Y ions serving as 6-c and the ligand as 8-c nodes) as shown in Fig. S7a.† We have also obtained an alternative straight rod (STR) net representation[32] because the standard **sea** net does not reflect the rod-MOF essence of the **HIAM-317** with clarity, although it may serve as a starting point for the search of analogous MOFs using the data from the TopCryst service[33] as described in full detail in the ESI† Methods. In the STR representation the biphenyl core of the $TCHB^{4-}$ ligand is represented as two linked 3-c nodes and the rods comprise carboxylate-connected Y^{3+} ions. The rods appear as zig-zag chains of nodes upon simplification and each of the nodes is 4-connected. The 3,4-c net obtained in such a way corresponds to the jeb topological type (Fig. S7b†). In addition, to comply with the point-of-extension (PE) approach described by O'Keeffe and coworkers[34] the metals are discarded and only the carbon atoms of the carboxylates serve as points of extension and form ladders connected by 4-c nodes representing the biphenyl ligand. The corresponding underlying net is the 4,4-c binodal **frl** net (Fig. S7c†).[35]

Stability

Powder X-ray diffraction (PXRD) analysis revealed that the pattern of the as-synthesized **HIAM-317** fully agreed with the simulated ones, suggesting the phase purity of the obtained material (Fig. S8†). In order to remove the non-bonded high boiling point solvents (DMF and water) residing inside the channels without disturbing the coordinated water arrays, solvent exchange by CH_2Cl_2 was employed. The thermogravimetric (TG) curve of the CH_2Cl_2-exchanged **HIAM-317** (CH_2Cl_2@**HIAM-317**) displays distinct two-step weight losses (Fig. S10†). The one before 100 °C corresponds to the loss of CH_2Cl_2, and the other at ~200 °C corresponds to the removal of coordinated water molecules (calculated: 3.7 wt%, experimentally observed: 3.67 wt%).

Activation of CH_2Cl_2@**HIAM-317** was initially carried out at 120 °C for 12 hours under vacuum. The process yielded **HIAM-317a**. Based on the TG curve, it was expected that under this activation condition, CH_2Cl_2 can be fully removed from the channels while leaving the coordinated water intact. Indeed, the morphology and crystallinity of the crystals were completely preserved upon activation, and subsequent structure analysis of **HIAM-317a** by SCXRD directly confirmed the preservation of coordinated water arrays. Further activation of CH_2Cl_2@**HIAM-317** was conducted at 300 °C under vacuum, yielding **HIAM-317b**. Apparently, it no longer contained any coordinated water arrays based on the TG profile. This was also supported by TG-MS analysis of CH_2Cl_2@**HIAM-317** which confirmed that the coordinated water molecules were removed at ~200 °C (Fig. S13†). Our attempt to determine the crystal structure of **HIAM-317b** by SCXRD failed due to cracking of the crystals upon heating at high temperature.[36,37] It is important to note that the PXRD patterns and morphology of **HIAM-317a** and **HIAM-317b** are identical to those of **HIAM-317**, indicating its

© 2024 The Author(s). Published by the Royal Society of Chemistry

Open Access Article. Published on 04 November 2024. Downloaded on 9/9/2025 4:14:33 AM. This article is licensed under a Creative Commons Attribution-NonCommercial 3.0 Unported Licence.

framework robustness (Fig. S2–S4 and S9†). Moreover, no notable structure flexibility was observed for **HIAM-317**.

Porosity characterization and single-component gas adsorption

Controllable activation of **HIAM-317** led to the formation of **HIAM-317a** and **HIAM-317b** with distinct pore dimensions and pore surface chemistry. This prompted us to explore their porosity and possible selective adsorption of alkenes/alkanes. The permanent porosity of **HIAM-317a** and **HIAM-317b** was analyzed by measuring N_2 adsorption at 77 K. As shown in Fig. 3a, **HIAM-317a** took up essentially no N_2. This is not surprising considering the ultra-narrow pore aperture of **HIAM-317a** because of the presence of coordinated water arrays. In contrast, **HIAM-317b** displayed a typical Type-I adsorption profile with saturated adsorption capacity of 145.29 $cm^3\ g^{-1}$ at $P/P_0 = 1$, yielding a Brunauer–Emmett–Teller (BET) surface area of 535 $m^2\ g^{-1}$. In the subsequent CO_2 adsorption measurements at 195 K, both **HIAM-317a** and **HIAM-317b** exhibited Type-I adsorption isotherms, with saturated uptake of 116.37 and 173.33 $cm^3\ g^{-1}$, respectively. The calculated BET surface area of **HIAM-317a** is 248 $m^2\ g^{-1}$. Furthermore, the pore size distribution curves are centered at 4.8 and 7.4 Å for **HIAM-317a** and **HIAM-317b**, respectively, consistent with the values determined by their crystal structure (Fig. 3b, inset).

The pore dimensions of **HIAM-317a** and **HIAM-317b** fall in the range that is well suited for alkene/alkane separation. Thus, we collected the single-component adsorption isotherms for C_2H_4, C_2H_6, C_3H_6, and C_3H_8 at ambient temperature. At 298 K, **HIAM-317a** showed kinetic sieving for both C_2H_4/C_2H_6 and C_3H_6/C_3H_8. It took up 16.62 $cm^3\ g^{-1}$ of C_2H_4 and 19.77 $cm^3\ g^{-1}$ of C_3H_6 at 1.0 bar. In contrast, its adsorption toward C_2H_6 was much slower with substantially lower adsorbed amount than that of C_2H_4, and C_3H_8 was fully excluded by the material with essentially no adsorption. The absorption ratio of C_3H_6/C_3H_8 is 23.2, which is at a high level among the reported adsorbents.[38–40] With coordinated water arrays removed from the channel, **HIAM-317b** demonstrated distinct adsorption behavior from that of **HIAM-317a** because of the notable change of pore dimensions and pore surface chemistry. **HIAM-317b** exhibited substantial adsorption toward all four hydrocarbon molecules without notable diffusion restrictions. At 298 K and 1 bar, the adsorption capacity of C_2H_6 was 45.08 $cm^3\ g^{-1}$, exceeding that of C_2H_4 (40.82 $cm^3\ g^{-1}$), displaying alkane-selective behavior. The IAST adsorption selectivity calculated for C_2H_6/C_2H_4 is 1.51 at 1 bar (Fig. S12†).[41] We also calculated isosteric heats of adsorption (Q_{st}) using adsorption isotherms at 298 K and 273 K.[42] The higher Q_{st} value for C_2H_6 (24.1 kJ mol^{-1}) than that of C_2H_4 (22.6 kJ mol^{-1}) confirmed the stronger interaction between the former and the channel of **HIAM-317b** (Fig. 3c). Interestingly, the adsorption selectivity for C3 is reversed. The adsorption capacities for C_3H_6 and C_3H_8 are 47.52 $cm^3\ g^{-1}$ and 38.12 $cm^3\ g^{-1}$, respectively, showing alkene-selective behavior (Fig. 3d and e). This was further confirmed by the Q_{st} of C_3H_6 (47.5 kJ mol^{-1}) and C_3H_8 (40.4 kJ mol^{-1}). These results indicate that **HIAM-317** serves as a highly tunable adsorbent and its adsorptive separation behavior can be tailored in a controllable manner by manipulating the coordinated water arrays in its channels.

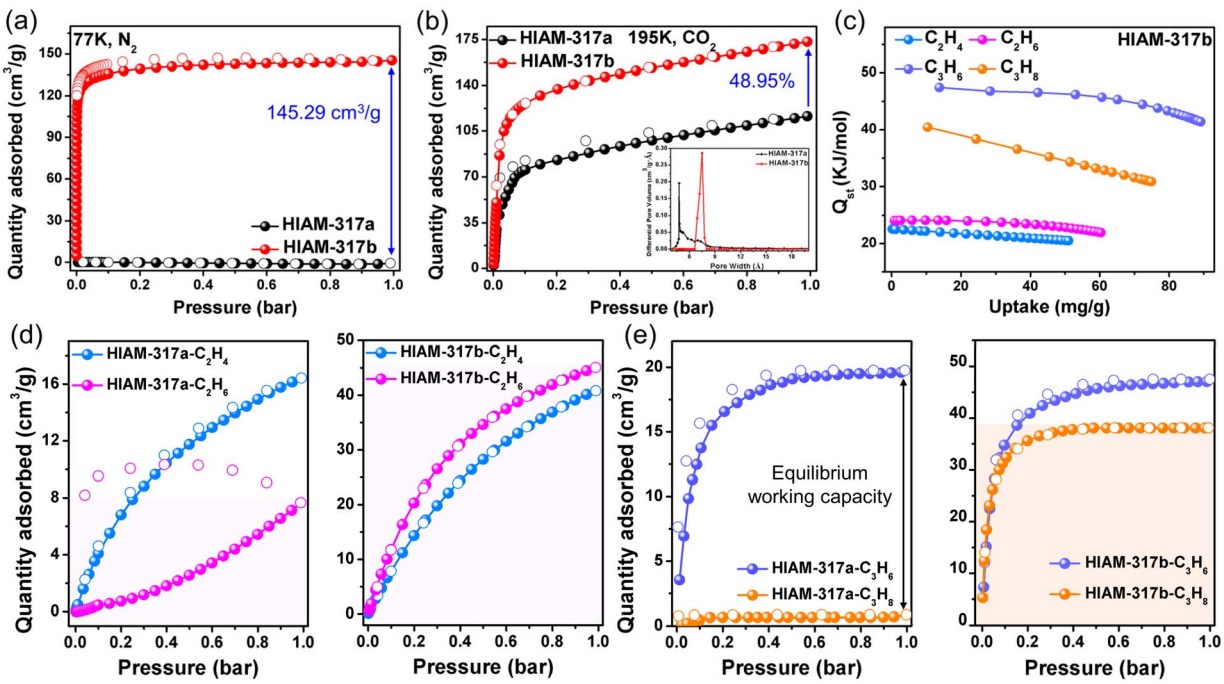

Fig. 3 (a) Adsorption isotherms of N_2 at 77 K; (b) adsorption isotherms of CO_2 at 195 K (insert: pore width of **HIAM-317a** and **HIAM-317b**); (c) the Q_{st} curves of C_2H_4, C_2H_6, C_3H_6, and C_3H_8 for **HIAM-317b**; (d) adsorption isotherms of C_2H_4 and C_2H_6 for **HIAM-317a** and **HIAM-317b** at 298 K; (e) adsorption isotherms of C_3H_6 and C_3H_8 for **HIAM-317a** and **HIAM-317b** at 298 K.

Open Access Article. Published on 04 November 2024. Downloaded on 9/9/2025 4:14:33 AM. This article is licensed under a Creative Commons Attribution-NonCommercial 3.0 Unported Licence.

Dynamic breakthrough experiments

To confirm the alkene/alkane separation capability of **HIAM-317a** and **HIAM-317b**, and the role of coordinated water arrays, alkene/alkane binary breakthrough experiments were conducted for equimolar mixtures of C_2H_4/C_2H_6 and C_3H_6/C_3H_8 at 298 K. The results of breakthrough measurements are fully consistent with the single-component adsorption isotherms. **HIAM-317a** exhibits a noticeable molecular sieving effect for both C_2H_4/C_2H_6 and C_3H_6/C_3H_8, with negligible dynamic adsorption for C_2H_6 and C_3H_8 and notably longer retention of their corresponding alkenes in the column. **HIAM-317b**, on the other hand, exhibits notable retention for all four gases. In the measurement of C_2H_4/C_2H_6, C_2H_4 eluted out first at the 30th minute, followed by the detection of C_2H_6. This validated its selective adsorption of ethane over ethylene. As expected, the measurement of C_3H_6/C_3H_8 displayed a different elution sequence. As shown in Fig. 4d, C_3H_8 was first detected at the outlet, and the elution of C_3H_6 was notably delayed, confirming the favored adsorption of propylene over propane. In equimolar alkane-alkene mixtures, the productivity of pure C_2H_6 (>99.99%) and C_3H_8 (>99.99%) is approximately 5.54×10^{-3} L kg^{-1} and 1.96 L kg^{-1}, respectively, by **HIAM-317a**. Meanwhile, **HIAM-317b** can produce high-purity C_2H_4 (>99.99%) at roughly 1.38×10^{-2} L kg^{-1}, effectively purifying approximately 2.5% of ethylene from the mixture, as well as C_3H_8 (>99.99%) at around 1.58 L kg^{-1}. These results experimentally confirmed the separation capability of **HIAM-317a** and **HIAM-317b** and align with the calculated breakthrough data (Fig. S16†), demonstrating the adjustable separation on a single adsorbent through pore structure engineering.

DFT calculation and molecular modeling

To gain a deeper insight into the underlying mechanisms of the different separation behavior and molecular–level interactions between guest molecules and the framework of **HIAM-317a** and **HIAM-317b**, DFT calculation and molecular simulation were performed.[43,44] First, the climbing-image nudged elastic band (cNEB) calculations were employed to evaluate the diffusion energy barrier of all four gases within the channels of **HIAM-317a**. As illustrated in Fig. 5, the energy barriers for alkanes (C_3H_8 and C_2H_6) are notably higher than those of alkenes (C_3H_6 and C_2H_4). This fully supports the gas adsorption results that **HIAM-317a** adsorbs alkenes while their corresponding alkanes can be barely adsorbed because of its limiting pore aperture. The molecular simulation results show that the coordination water array in the pore is not only the main reason for regulating the adsorption mechanism transformation, but also the main adsorption site (Fig. S17†) for alkenes. In contrast, the main binding sites in **HIAM-317b** are located nearby the carboxyl oxygen atoms as well as the neighboring benzene ring. Compared to C_2H_4, C_2H_6 binds to the framework with stronger

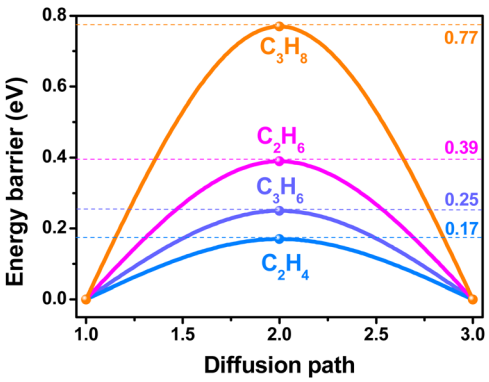

Fig. 5 Energy barrier for C_2H_4, C_2H_6, C_3H_6 and C_3H_8 to diffuse into the channels of HIAM-317a.

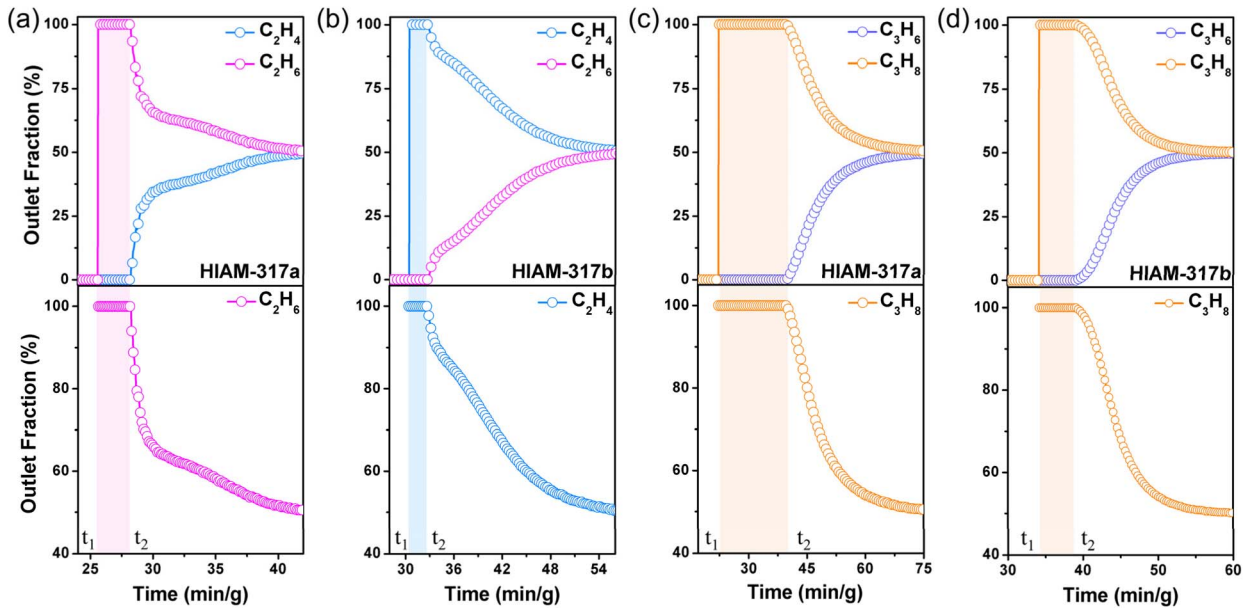

Fig. 4 The dynamic breakthrough curves of equimolar C_2H_4/C_2H_6 mixtures for HIAM-317a (a) and HIAM-317b (b) and equimolar C_3H_6/C_3H_8 mixtures for HIAM-317a (c) and HIAM-317b (d) at 298 K.

© 2024 The Author(s). Published by the Royal Society of Chemistry

Open Access Article. Published on 04 November 2024. Downloaded on 9/9/2025 4:14:33 AM.
This article is licensed under a Creative Commons Attribution-NonCommercial 3.0 Unported Licence.

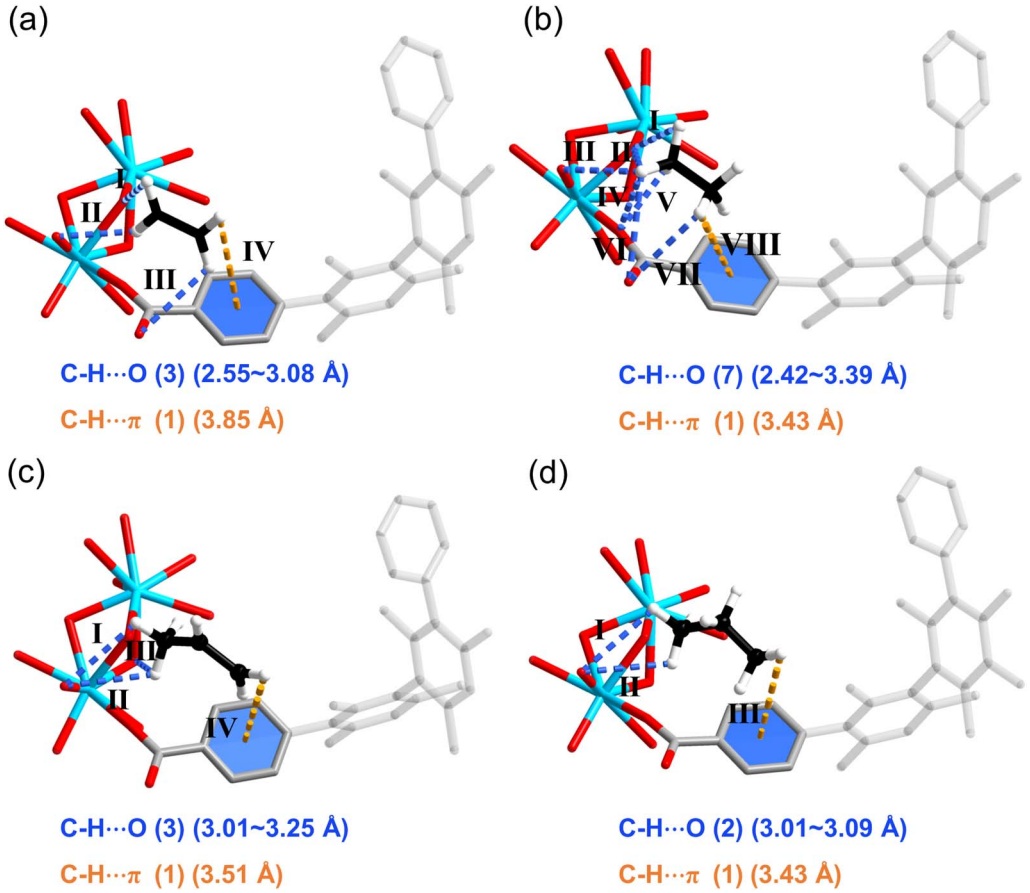

Fig. 6 The preferential adsorption sites of **HIAM-317b** for (a) C_2H_4, (b) C_2H_6, (c) C_3H_6 and (d) C_3H_8, the C–H···π and C–H···O interactions are presented by orange and blue dashed lines respectively.

interaction due to its more C–H binding contacts with the framework through seven C–H···O (2.42–3.39 Å) bonds (Fig. 6a and b). Interestingly, C_3H_6 exhibits notable contacts with the adjacent benzene ring through C–H···π interaction (C–H···π distance: 3.51 Å). In addition, it also has a closer contact with the carboxyl oxygens (C–H···O: 3.01–3.25 Å) compared to that of C_3H_8 (Fig. 6c). This explains the preferential adsorption of C_3H_6 over C_3H_8 in **HIAM-317b**. The calculated binding energies (ΔE) of C_2H_4, C_2H_6, C_3H_6, and C_3H_8 on **HIAM-317b** are 27.64, 32.58, 51.84 and 44.93 kJ mol^{-1}, respectively (Fig. S18†), which are consistent with the trends of Q_{st} obtained from adsorption isotherms.

Conclusions

In this study, we present a strategy to engineer the pore structure of an yttrium-based MOF $[Y_2(TCHB)(OH)_2 \cdot 2H_2O]$ (**HIAM-317**) *via* coordinated water arrays, and controllable separation of alkenes and alkanes by the two forms of **HIAM-317** (with and without coordinated water molecules). Our single-component adsorption, multicomponent breakthrough measurements, and theoretical calculations and simulations suggest that the coordinated water arrays serve as a regulatory factor for its effective pore aperture and pore surface chemistry. In the presence of coordinated water, **HIAM-317a** splits ethylene/ethane and propylene/propane because of its suitable pore aperture. In the absence of coordinated water, **HIAM-317b** exhibits thermodynamically driven ethane-selective separation of ethylene/ethane and propylene-selective separation of propylene/propane. The distinct selectivity for C2 and C3 alkenes/alkanes originates from the oxygen-rich pore surface and the adsorbate-dependent recognition mechanisms. We demonstrate the practice of all three separation mechanisms on a single adsorbent by engineering its pore structure.

Data availability

The data supporting this article have been included as part of the ESI.†

Author contributions

H. Wang, G.-P. Yang, and J. Li designed the project. L.-L. Ma synthesized the compounds, analyzed the PXRD, adsorption, and breakthrough test results, and carried out the calculations and simulations. K. Zhou carried out the single-crystal X-ray diffraction experiments and analyzed the data. X. Zhou, J. Liu, J. Miao and S. Li conducted and analyzed the stability test

Open Access Article. Published on 04 November 2024. Downloaded on 9/9/2025 4:14:33 AM. This article is licensed under a Creative Commons Attribution-NonCommercial 3.0 Unported Licence.

results. P. Zolotarev and D. Proserpio analyzed the structure and topology. L.-L. Ma, H. Wang, G.-P. Yang, Y.-Y. Wang, and J. Li wrote the first draft. All authors contributed to the discussion and revision of the manuscript.

Conflicts of interest

There are no conflicts to declare.

Acknowledgements

The authors acknowledge the support of this work by the Shenzhen Science and Technology Program (KCXFZ20211020163818026), National Natural Science Foundation of China (22478251, 22071194, and 22371225), and the U.S. Department of Energy, Basic Energy Sciences, Division of Materials Sciences and Engineering (Grant No. DE-SC0019902). DMP and PNZ thank the MUR for the grant PRIN2020 "Nature Inspired Crystal Engineering (NICE)" and Prof. Vladislav A. Blatov at the Samara Center for Theoretical Materials Science for providing the free ToposPro software (**https://topospro.com**).

Notes and references

1 S. A. Chernyak, M. Corda, J.-P. Dath, V. V. Ordomsky and A. Y. Khodakov, Light olefin synthesis from a diversity of renewable and fossil feedstocks: state-of the-art and outlook, *Chem. Soc. Rev.*, 2022, **51**, 7994–8044.

2 V. F. D. Martins, A. M. Ribeiro, M. G. Plaza, J. C. Santos, J. M. Loureiro, A. F. P. Ferreira and A. E. Rodrigues, Gas-phase simulated moving bed: Propane/propylene separation on 13X zeolite, *J. Chromatogr. A*, 2015, **1423**, 136–148.

3 I. Amghizar, L. A. Vandewalle, K. M. Van Geem and G. B. Marin, New Trends in Olefin Production, *Engineer*, 2017, **3**, 171–178.

4 P. Group, Global market for ethylene propylene manufacturing to reach $5.4B by 2023, *Processing*, 2018, **31**, 8.

5 R. B. Eldridge, Olefin/Paraffin Separation Technology: A Review, *Ind. Eng. Chem. Res.*, 1993, **32**, 2208–2212.

6 S. M. Sadrameli, Thermal/catalytic cracking of liquid hydrocarbons for the production of olefins: a state-of-the-art review II: catalytic cracking review, *Fuel*, 2016, **173**, 285–297.

7 W. J. Koros and R. P. Lively, Water and beyond: expanding the spectrum of large-scale energy efficient separation processes, *AlChE J.*, 2012, **58**, 2624–2633.

8 S. Mukherjee, D. Sensharma, K.-J. Chen and M. J. Zaworotko, Crystal engineering of porous coordination networks to enable separation of C2 hydrocarbons, *Chem. Commun.*, 2020, **56**, 10419–10441.

9 D. S. Sholl and R. P. Lively, Seven chemical separations to change the world, *Nature*, 2016, **532**, 437.

10 S. Chu, Y. Cui and N. Liu, The path towards sustainable energy, *Nat. Mater.*, 2016, **16**, 16–22.

11 Y. Chai, X. Han, W. Li, S. Liu, S. Yao, C. Wang, W. Shi, I. da-Silva, P. Manuel, Y. Cheng, L. D. Daemen, A. J. Ramirez-Cuesta, C. C. Tang, L. Jiang, S. Yang, N. Guan and L. Li, Control of zeolite pore interior for chemoselective alkyne/olefin separations, *Science*, 2020, **368**, 1002–1006.

12 Y. Peng, H. Xiong, P. Zhang, Z. Zhao, X. Liu, S. Tang, Y. Liu, Z. Zhu, W. Zhou, Z. Deng, J. Liu, Y. Zhong, Z. Wu, J. Chen, Z. Zhou, S. Chen, S. Deng and J. Wang, Interaction-selective molecular sieving adsorbent for direct separation of ethylene from senary C2-C4 olefin/paraffin mixture, *Nat. Commun.*, 2024, **15**, 625.

13 H. S. Lee, N. S. Kim, D. i. Kwon, S. K. Lee, M. Numan, T. Jung, K. Cho, M. Mazur, H. S. Cho and C. Jo, Post-Synthesis Functionalization Enables Fine-Tuning the Molecular-Sieving Properties of Zeolites for Light Olefin/Paraffin Separations, *Adv. Mater.*, 2021, **33**, 2105398.

14 R. B. Lin, L. Li, H. L. Zhou, H. Wu, C. He, S. Li, R. Krishna, J. Li, W. Zhou and B. Chen, Molecular sieving of ethylene from ethane using a rigid metal-organic framework, *Nat. Mater.*, 2018, **17**, 1128–1133.

15 Q. Dong, Y. Huang, J. Wan, Z. Lu, Z. Wang, C. Gu, J. Duan and J. Bai, Confining Water Nanotubes in a $Cu_{10}O_{13}$-Based Metal-Organic Framework for Propylene/Propane Separation with Record-High Selectivity, *J. Am. Chem. Soc.*, 2023, **145**, 8043–8051.

16 A. Cadiau, K. Adil, P. M. Bhatt, Y. Belmabkhout and M. Eddaoudi, A metal-organic framework–based splitter for separating propylene from propane, *Science*, 2016, **353**, 137–140.

17 J. Liu, K. Zhou, S. Ullah, J. Miao, H. Wang, T. Thonhauser and J. Li, Precise Pore Engineering of fcu-Type Y-MOFs for One-Step C_2H_4 Purification from Ternary $C_2H_6/C_2H_4/C_2H_2$ Mixtures, *Small*, 2023, **19**, 2304460.

18 L. Yu, X. Han, H. Wang, S. Ullah, Q. Xia, W. Li, J. Li, I. da Silva, P. Manuel, S. Rudic, Y. Cheng, S. Yang, T. Thonhauser and J. Li, Pore Distortion in a Metal-Organic Framework for Regulated Separation of Propane and Propylene, *J. Am. Chem. Soc.*, 2021, **143**, 19300–19305.

19 B. Liang, X. Zhang, Y. Xie, R.-B. Lin, R. Krishna, H. Cui, Z. Li, Y. Shi, H. Wu, W. Zhou and B. Chen, An Ultramicroporous Metal–Organic Framework for High Sieving Separation of Propylene from Propane, *J. Am. Chem. Soc.*, 2020, **142**, 17795–17801.

20 X. W. Gu, J. X. Wang, E. Wu, H. Wu, W. Zhou, G. Qian, B. Chen and B. Li, Immobilization of Lewis Basic Sites into a Stable Ethane-Selective MOF Enabling One-Step Separation of Ethylene from a Ternary Mixture, *J. Am. Chem. Soc.*, 2022, **144**, 2614–2623.

21 F. Xie, H. Wang and J. Li, Microporous metal–organic frameworks for the purification of propylene, *J. Mater. Chem. A*, 2023, **11**, 12425–12433.

22 W. Xie, L. Yang, J. Zhang and X. Zhao, The Adsorptive Separation of Ethylene from C2 Hydrocarbons by Metal-Organic Frameworks, *Chem.–Eur. J.*, 2023, **29**, e202300158.

23 Y.-L. Li, E. V. Alexandrov, Q. Yin, L. Li, Z.-B. Fang, W. Yuan, D. M. Proserpio and T.-F. Liu, Record Complexity in the

© 2024 The Author(s). Published by the Royal Society of Chemistry

Open Access Article. Published on 04 November 2024. Downloaded on 9/9/2025 4:14:33 AM. This article is licensed under a Creative Commons Attribution-NonCommercial 3.0 Unported Licence.

Polycatenation of Three Porous Hydrogen-Bonded Organic Frameworks with Stepwise Adsorption Behaviors, *J. Am. Chem. Soc.*, 2020, **142**, 7218–7224.

24 J. Fu, J. Y. Liu, G. H. Zhang, Q. H. Zhu, S. L. Wang, S. Qin, L. He and G. H. Tao, Boost of Gas Adsorption Kinetics of Covalent Organic Frameworks *via* Ionic Liquid Solution Process, *Small*, 2023, **19**, 2302570.

25 X. Li, K. Chen, R. Guo and Z. Wei, Ionic Liquids Functionalized MOFs for Adsorption, *Chem. Rev.*, 2023, **123**, 10432–10467.

26 W. Fan, X. Zhang, Z. Kang, X. Liu and D. Sun, Isoreticular chemistry within metal–organic frameworks for gas storage and separation, *Coord. Chem. Rev.*, 2021, **443**, 213968.

27 O. M. Yaghi, M. O'Keeffe, N. W. Ockwig, H. K. Chae, M. Eddaoudi and J. Kim, Reticular synthesis and the design of new materials, *Nature*, 2003, **423**, 705–714.

28 X. Zhang, Y. Li and J.-R. Li, Metal–organic frameworks for multicomponent gas separation, *Trends Chem.*, 2024, **6**, 22–36.

29 J.-R. Li, J. Sculley and H.-C. Zhou, Metal–Organic Frameworks for Separations, *Chem. Rev.*, 2012, **112**, 869–932.

30 V. A. Blatov, A. P. Shevchenko and D. M. Proserpio, Applied Topological Analysis of Crystal Structures with the Program Package ToposPro, *Cryst. Growth Des.*, 2014, **14**, 3576–3586.

31 C. Bonneau, M. O'Keeffe, D. M. Proserpio, V. A. Blatov, S. R. Batten, S. A. Bourne, M. S. Lah, J.-G. Eon, S. T. Hyde, S. B. Wiggin and L. Öhrström, Deconstruction of Crystalline Networks into Underlying Nets: Relevance for Terminology Guidelines and Crystallographic Databases, *Cryst. Growth Des.*, 2018, **18**, 3411–3418.

32 L. S. Xie, E. V. Alexandrov, G. Skorupskii, D. M. Proserpio and M. Dincă, Diverse π–π stacking motifs modulate electrical conductivity in tetrathiafulvalene-based metal–organic frameworks, *Chem. Sci.*, 2019, **10**, 8558–8565.

33 A. P. Shevchenko, A. A. Shabalin, I. Y. Karpukhin and V. A. Blatov, Topological representations of crystal structures: generation, analysis and implementation in the TopCryst system, *Sci. Technol. Adv. Mater.: Methods*, 2022, **2**, 250–265.

34 A. Schoedel, M. Li, D. Li, M. O'Keeffe and O. M. Yaghi, Structures of Metal–Organic Frameworks with Rod Secondary Building Units, *Chem. Rev.*, 2016, **116**, 12466–12535.

35 W. Fan, X. Wang, B. Xu, Y. Wang, D. Liu, M. Zhang, Y. Shang, F. Dai, L. Zhang and D. Sun, Amino-functionalized MOFs with high physicochemical stability for efficient gas storage/separation, dye adsorption and catalytic performance, *J. Mater. Chem. A*, 2018, **6**, 24486–24495.

36 S. Materazzi, Mass Spectrometry Coupled to Thermogravimetry (TG-MS) for Evolved Gas Characterization: A Review, *Appl. Spectrosc. Rev.*, 1998, **33**, 189–218.

37 P. Yuan, D. Yang, R. Wang, N. Gong, L. Zhang, Y. Lu and G. Du, Characterization of a New Solvatomorph of Drospirenone by Thermogravimetry–Mass Spectrometry Combined with Other Solid-State Analysis Methods, *ACS Omega*, 2020, **5**, 25289–25296.

38 Y. Wang, N. Y. Huang, X. W. Zhang, H. He, R. K. Huang, Z. M. Ye, Y. Li, D. D. Zhou, P. Q. Liao, X. M. Chen and J. P. Zhang, Selective Aerobic Oxidation of a Metal–Organic Framework Boosts Thermodynamic and Kinetic Propylene/Propane Selectivity, *Angew. Chem., Int. Ed.*, 2019, **58**, 7692–7696.

39 H. Zeng, M. Xie, T. Wang, R. J. Wei, X. J. Xie, Y. Zhao, W. Lu and D. Li, Orthogonal-array dynamic molecular sieving of propylene/propane mixtures, *Nature*, 2021, **595**, 542–548.

40 X. Wang, R. Krishna, L. Li, B. Wang, T. He, Y.-Z. Zhang, J.-R. Li and J. Li, Guest-dependent pressure induced gate-opening effect enables effective separation of propene and propane in a flexible MOF, *Chem. Eng. J.*, 2018, **346**, 489–496.

41 S. Sharma, S. R. G. Balestra, R. Baur, U. Agarwal, E. Zuidema, M. S. Rigutto, S. Calero, T. J. H. Vlugt and D. Dubbeldam, RUPTURA: simulation code for breakthrough, ideal adsorption solution theory computations, and fitting of isotherm models, *Mol. Simul.*, 2023, **49**, 893–953.

42 A. Nuhnen and C. Janiak, A practical guide to calculate the isosteric heat/enthalpy of adsorption *via* adsorption isotherms in metal–organic frameworks, MOFs, *Dalton Trans.*, 2020, **49**, 10295–10307.

43 G. Kresse and J. Furthmüller, Efficient iterative schemes for *ab initio* total-energy calculations using a plane-wave basis set, *Phys. Rev. B: Condens. Matter Mater. Phys.*, 1996, **54**, 11169–11186.

44 G. Kresse and D. Joubert, From ultrasoft pseudopotentials to the projector augmented-wave method, *Phys. Rev. B: Condens. Matter Mater. Phys.*, 1999, **59**, 1758–1775.

© 2024 The Author(s). Published by the Royal Society of Chemistry